

Assessing California's Thomas Wildfire and Montecito's Debris-Flow Risk with Sentinel-2 Imagery and the High-Resolution Rapid Refresh Model

Erik M. Neemann

Introduction

Wildfire is a common hazard faced by many communities in the western US. In some cases, an additional landslide or debris-flow hazard may follow the occurrence of wildfire when vulnerable locations experience intense rainfall events. This further threatens communities with possible loss of life and significant property damage. In the future, a changing climate may increase exposure to these hazards due to a potential increase in wildfires and high-intensity precipitation events (Melillo et al. 2014). A case study will be presented to examine the Thomas Fire in southern California and subsequent debris-flows in Montecito. This study leverages remotely sensed imagery to identify wildfire burn severity and locations at risk of debris-flows based on a digital elevation model (DEM), soil erodibility, and model forecast precipitation data. A change detection exercise and supervised classification techniques are also applied to the imagery for the purposes of burned area and severity identification. The primary motivation for this work is to help answer the following research questions:

- Can analysis of remotely sensed imagery, combined with DEM, soil, and precipitation data, help identify burn areas and debris-flow risk following the Thomas wildfire?
- Does the application of model-based precipitation forecasts further improve the debris-flow risk assessment for the Montecito area?

The Thomas fire burned areas of Ventura and Santa Barbara counties in southern California between ignition on 4 December 2017 and containment on 12 January 2018. It erupted in early December as high pressure over the Great Basin fueled strong Santa Ana winds and dry conditions. When it was finally contained in mid-January 2018, the Thomas Fire had burned 281,893 acres, making it the largest California wildfire in modern history. The fire caused the evacuation of more than 100,000 people and destroyed over 1300 structures (Cal Fire 2018). The large swath of burn-scarred land immediately became vulnerable to mudslides and debris-flows. On 9 January 2018, an atmospheric river event brought tremendous precipitation to southern California and 13.7 mm (0.54 in) of rain fell in just 5 minutes on Montecito and the nearby mountains to the north (National Weather Service 2018). The resulting debris-flows killed 21 people, destroyed 166 structures, and damaged 395 additional structures (Cal Fire 2018). The photos in Figure 1 demonstrate some of the damage that resulted from the debris-flows. Much of the region ended up with 7-15 cm (2.75-5.9 in) of rain in just 2 days. The combination of recent wildfires, intense precipitation, and terrain characteristics (slope severity and soil properties) generated the devastating debris-flows. A map of the primary study area for this research is depicted in Figure 2.

Relevant Literature

In recent decades, dozens of articles have been added to the scientific literature, covering both wildfire severity identification through remote sensing analysis and debris-flow probability prediction following wildfire. This paper will focus on techniques used by two specific studies. An article by Brewer et al. in 2005 investigated several methods for classifying wildfire severity using Landsat Thematic Mapper (TM) imagery. These methods include image differencing and ratioing, principal component analysis, and artificial neural networks (ANN). Most of these techniques involved the analysis of pre- and post-fire imagery, with the exception being one ANN technique, which relied solely on post-fire imagery. Brewer found that calculating the difference normalized burn ratio (dNBR) from TM imagery proved to be most consistent, robust, and simple/straight-forward method for classifying and mapping wildfire burn severity (Brewer et al. 2005). For this reason, it was identified as a good choice for operational applications in the continental U.S. and was used in this study to characterize burned areas and their severity.

Another article, by Staley et al. in 2016, focused on calculating rainfall intensity thresholds for post-fire debris-flows in the western US. Four logistic regression approaches for predicting debris-flow probability were compared and validated against a database of 611 records.

Different rainfall intensity duration thresholds of 15, 30, 45, and 60 minutes were also examined for each model. The “M1” model, which is based on terrain steepness, burn severity, soil erodibility, and rainfall intensity, demonstrated the best performance in predicting debris-flow occurrence. Further, all models performed best using the 15-min rainfall intensity threshold (Staley et al. 2016). With this in mind, the M1 model and 15-min rainfall threshold is used in this study to calculate debris-flow probability.

Data

All data used in this research came from free, publicly-available sources. Satellite imagery from the Sentinel-2 Multispectral Imager (MSI) was gathered from the European Space Agency via Google Earth Engine. The MSI has 13 bands spanning the visible to shortwave infrared wavelengths at variable spatial resolutions of 10, 20, and 60m (Table 1). Bands from Table 1 that are highlighted in red were used for normalized burn ratio (NBR) calculations, which will be described in the next section. Band 12 and Band 8A were selected because they were the bands that most closely resembled Landsat TM bands, while matching each other in spatial resolution. All of the bands in Table 1 that are highlighted in green and red were used for supervised classification. This subset of bands was selected due to their higher resolution; the 60 m bands were not used. Finally, top of the atmosphere (TOA) reflectances that are publically distributed for Sentinel-2 data were used in the analysis. Some consideration was given to using surface reflectances, but atmospherically corrected imagery is not currently distributed, and manually performing atmospheric correction proved to be a very complex process for MSI data. Further, TOA reflectances have been routinely used for years to identify burn severity in operational applications used by the U.S. Forest Service (P. Dennison, personal communication, March 12, 2018). An example of Sentinel-2 imagery from after the Thomas Fire, taken on 22 January, 2018 is shown in Figure 3.

Digital Elevation Model (DEM) data was collected from the USGS National Map at 1/9 arc-second resolution (~10 m). Soil erodibility data came from the Natural Resources Conservation Service's State Soil Geographic Data Base. Precipitation observations were gathered from the National Weather Service and precipitation forecasts from the operational High-Resolution Rapid Refresh (HRRR) model were downloaded from the HRRR Archive at the University of Utah. The fire perimeter and watershed outlets (pour points) were derived from USGS data. The debris-flow polygons used for subjective validation were pulled from a web map produced by the Santa Barbara Independent. All additional boundaries and GIS data were acquired from the UCLA Geoportal.

Band	Resolution	Wavelength	Description
B1	60 m	443 nm	Aerosols
B2	10 m	490 nm	Blue
B3	10 m	560 nm	Green
B4	10 m	665 nm	Red
B5	20 m	705 nm	Red Edge 1
B6	20 m	740 nm	Red Edge 2
B7	20 m	783 nm	Red Edge 3
B8	10 m	842 nm	NIR
B8A	20 m	865 nm	Red Edge 4
B9	60 m	940 nm	Water vapor
B10	60 m	1375 nm	Cirrus
B11	20 m	1610 nm	SWIR 1
B12	20 m	2190 nm	SWIR 2

Table 1: Sentinel-2 MSI bands

Methods

NBR and Change Detection

The first methodology that will be discussed is the NBR calculation and its use for change detection on the Thomas Fire. Sentinel-2 imagery of southern California was collected for pre-fire (3 December 2017) and post-fire (22 January 2018) conditions. The NBR (Brewer 2005) was then calculated for each image from Band 12 (SWIR, 2190 nm) and Band 8A (NIR, 865 nm) TOA reflectances using the formula below:

$$NBR = \frac{NIR - SWIR}{NIR + SWIR}$$

A differenced NBR (dNBR) was generated from the pre- and post-fire NBR data to identify burn severity resulting from the Thomas Fire. To perform the burn severity change detection, an additional dNBR image was generated from the pre-fire image and a post-fire image, dated 28 March 2018. The original dNBR image (22 January 2018) was then subtracted from the later

dNBR image (new image - old image) to determine areas of dNBR change, indicative of regrowth in the fire region from late January to late March 2018.

Debris-Flow Probability

The second methodology used the aforementioned NBR data and several additional GIS datasets to replicate the USGS debris-flow probability model. All of these datasets required some level of pre-processing prior to their use in the model. The dNBR burn severity data had to be placed into classes of low, moderate, and high burn severity. The severity thresholds for moderate (> 0.35) and high (> 0.65) burns were set as the average respective threshold from California fires in 2015, according to data from Monitoring Trends in Burn Severity (MTBS; Eidenshink 2007). This number was then rounded up to the next multiple of 0.05, to ensure a conservative threshold that didn't overestimate burn severity.

The DEM data was used in a hydrology workflow to delineate primary streams and watershed boundaries. First, a filled DEM was created and used to build a flow direction raster, followed by a flow accumulation raster. The flow accumulation data was then filtered to contributing areas greater than 1000 sq m to determine primary streams. Next, the USGS pour point data were snapped to the manually-created streams. Finally, the flow direction and pour point data were used to calculate watershed boundaries and the raster output was converted into a polygon feature class. These watershed polygons would later be used to calculate average “upstream area” values for the inputs in the USGS debris-flow model.

A slope raster was also built from the 10 m DEM dataset and the STATSGO fine fraction soil erodibility data (KF-Factor) was converted from polygons to raster. For precipitation data, the 0500 UTC run of the operational HRRR model was used, with hourly rainfall at the end of forecast hour 08, valid 1300 UTC. This output was selected because it was representative of observed rainfall, though the timing was off by 75-90 min from the actual rainfall maximum (~1130 UTC) for the Montecito event. It also represented real-time weather model data that would have been available approximately 6 hours before the debris-flow event occurred and could have been used for short-notice evacuation decisions. Additional, uniform rainfall thresholds were also used as model inputs, as discussed below.

Once the foundational data was prepared, debris-flow probabilities for the 9 January 2018 Montecito event were calculated based on the logistic regression approach employed by the USGS (Staley et al. 2016), where statistical likelihood of debris-flow occurrence, P, is:

$$P = \frac{e^\chi}{1 + e^\chi}$$

Further, χ is determined by the link function:

$$\chi = \beta + C_1 TR + C_2 FR + C_3 SR$$

The parameters in the link function are described in Table 2. Each of these parameters, and the probability of debris-flow occurrence was calculated at the watershed level. A diagram of this model methodology is also shown in Figure 4. This logistic regression approach was used to

model predicted debris-flow probability based on a common USGS rainfall threshold (6 mm in 15 min), actual observations in Montecito (13.7 mm in less than 15 min), and rainfall rates converted from HRRR hourly accumulated precipitation forecasts (~1.0-8.7 mm in 15 min) valid within 2 hours of the observed debris-flows. The use of high-resolution weather model data as the precipitation input for a debris-flow model appears to be a novel method that hasn't really been explored in the scientific literature.

Parameter	Value
β	-3.63, empirically defined coefficient
C_1	0.41, empirically defined coefficient
T	Proportion upstream area burned at moderate or high severity with slope gradient ≥ 23 degrees
R	15-minute rainfall accumulation, in mm
C_2	0.67, empirically defined coefficient
F	Mean upstream dNBR
C_3	0.70, empirically defined coefficient
S	Mean upstream Soil KF-Factor (fine-earth soil erodibility)

Table 2: Link function parameters

Debris-flow probabilities are evaluated by comparing results of the HRRR-based rainfall model to the uniform rainfall model used by USGS. Additionally, the methods are evaluated by quantifying the percentage of watersheds that exceed various probability thresholds. The results are also subjectively compared based on the spatial distribution of high-probability watersheds and the location of actual damage reports in the Montecito area.

Supervised Classification

The final analysis method employed in this study was the supervised classification of post-fire Sentinel-2 MSI imagery using the ENVI software package. This was initially performed with four classes (burned area, vegetation, water, and urban), but a fifth class was added to capture soil and non-photosynthetic vegetation (NPV). Working with such a large Sentinel-2 image (9.9 million pixels), each training region of interest (ROI) contained at least 6 thousand pixels. A maximum likelihood classifier was used to produce both 4- and 5-class images. An additional 5-class image was created with a multi-layer perceptron Neural Network (NN) classifier available in ENVI. The NN used a logistic activation function and 1 hidden layer with 1000 training iterations. Moderate training contribution and momentum values (0.5) were used, with a low training rate (0.1). A minimum activation threshold of 0.05 allowed some pixels to remain unclassified if their fuzzy membership value was below that threshold. The subset of MSI bands, highlighted in red and green in Table 2, was used to limit the classification to only higher-resolution 10 and 20 m data and remove the influence of aerosols, water vapor, and cirrus clouds from the analysis.

The classified images were subjectively evaluated by comparing the results from each classification to one another and SWIR imagery. This was done for both a large-scale view and by zooming in to specific locations. Further, accuracy metrics and confusion matrices were calculated using independent reference ROIs within the scene. While the reference and training ROIs did not overlap, the reference ROIs were taken from locations that were relatively clean and unambiguous. As discussed later, this may have artificially inflated the accuracy scores.

Results/Discussion

NBR and Change Detection

Results from the NBR (and dNBR) calculations for the Thomas Fire indicate a clear delineation of the burn scar area (Figure 5). The Thomas Fire burn region was readily detectable by visually comparing pre- and post-fire SWIR imagery, but dNBR did a good job of quantifying the burn severity. When looking closely at the results, some non-burned areas are also highlighted to the southeast of the burn scar, which are likely the result of agricultural activity and harvesting. However, the coherency of the burned area and the spatial patterns associated with non-burned features make it rather straightforward for even an untrained eye to effectively use the dNBR results. The quantification also proved useful for thresholding moderate and high burn severity areas for inclusion in the debris-flow probability model.

Change detection on the dNBR images from January and March helped identify areas in recovery, but results were mixed compared to the dNBR images themselves. For example, the southern and southeastern portion of the burn scars showed negative dNBR change values, indicative of some improvement or regrowth (Figure 6). This improvement also aligns fairly well with areas of relatively low burn severity, as identified by the original dNBR image (Figure 5), which are more likely to recover faster. On the other hand, there are a few areas showing spurious positive changes in dNBR, which indicate an increase in burn severity from the original 22 January 2018 image. This can be seen just north of the San Ynez Mountains ridgeline, south of the burn scar, and in the northern portion of the image. Since no additional fires burned in the region between January and March, these errors are largely attributed to differences in time of year, sun angle, and shadows. This is likely a case where atmospheric correction may have led to improved results. Overall, with some interpretation and knowledge of the event, the change detection method using dNBR images still appears to be a useful method for monitoring burn recovery.

If time allowed, an additional NBR calculation with Band 8 would have been conducted and compared with the results from Band 8A. The spectral center of Band 8 aligns more closely to the Landsat TM NIR Band 4, which is commonly used for NBR calculations. However, a switch to Sentinel-2 Band 8 would also require resampling from 10 to 20 m to match the coarser SWIR 2 band (B12). It is unknown if using the different NIR band would significantly impact the results of this study (both NBR and debris-flow probability calculations), but further investigation may prove valuable. As mentioned previously, atmospheric correction was not performed on the Sentinel-2 data and TOA reflectances were used to calculate NBR. While surface reflectance data are not readily distributed (as they often are with Landsat data), a more

rigorous methodology would be to perform atmospheric correction on each image prior to NBR and dNBR calculation. This may also result in greater fidelity of the change detection results and is recommended as further research. Finally, best results from NBR calculations are typically realized with imagery obtained as soon after the fire as possible. However, because the Thomas Fire burned for so long (40 days), some of the region likely stopped burning 6 weeks prior to the post-fire image on 22 January 2018. This was partly due to the length of the active fire, but also due to the desire to capture very clean images, with as little high cloud cover as possible. It should also be noted that the post-fire image used to calculate NBR for the debris-flow model would not have been available prior to the debris-flow event (9 January 2018). While it's not expected to have significantly impacted this study, a minor difference in results may be detectable with atmospherically correct images captured closer to the fire's containment, or even prior to full containment.

Debris-Flow Probability

The logistic regression approach successfully identified the debris-flow threat posed by the Thomas Fire to Montecito for the 9 January 2018 storm. All three models indicated an elevated threat ($P \geq 0.5$) for the watersheds above Montecito. When observed rainfall totals from Montecito on 9 January (13.7 mm in 15 min) were used in the model, it indicated $P > 0.99$ for debris-flows (not shown). This indicates how incredible the observed rainfall intensity was for that event and demonstrates the model's ability to capture very high debris-flow probability for such an extreme event. The common USGS uniform rainfall threshold of 6 mm in 15 minutes, also identified the high threat, generally with $0.591 < P < 0.798$ in the Montecito area (Figure 7). Additionally, forecasts from the HRRR model demonstrated intense rainfall leading to $0.663 < P < 0.882$ in the watersheds above Montecito. Predictions based on HRRR data also generated better spatial results for the entire Thomas Fire region, with the eastern portions of the burn scar showing low debris-flow probability as a reflection of decreased rainfall intensity there (Figure 7).

Overall, the spatially-varying debris-flow probabilities generated with HRRR model data decreased the percentage of high-probability watersheds, as shown in Table 3 below. When compared to the uniform precipitation probabilities, the added information from the HRRR model forecasts appear useful in isolating the greatest debris-flow threat, as opposed to generalizing high probabilities over a large area (Figure 7 bottom). If extended to other events, this could help reduce false alarms, constrain evacuation regions, modify response plans, and stage resources for recovery efforts.

Debris-Flow Threshold	Uniform 6 mm rainfall	HRRR-based rainfall
Probability > 0.4	60.90%	28.40%
Probability > 0.6	40.80%	16.90%
Probability > 0.8	21.60%	8.40%

Table 3: Percent of watersheds with debris-flow probability greater than given threshold

Closer inspection of the Montecito area, shows the HRRR-based probabilities accurately characterized the debris-flow hazard in the watersheds above the town, which feed the primary streams. All 561 structures that were damaged or destroyed in the event were located in the purple damage report area of Figure 8. The location of these damage reports fits closely with the primary streams that flow out of the high-risk watersheds, as identified by the logistic regression model.

The HRRR model data used in this study was limited to a handful of forecast hours from the operational 0500 UTC model run. If more time were available, additional forecast hours and several model runs would have been examined to most appropriately capture the event. In most cases, emergency management decisions aren't made based on output from a single weather model run. With this in mind, it would be especially useful to use an ensemble of several weather model runs as an input to the debris-flow model. This is a study limitation that could be improved upon in further research. Regardless, the results shown here indicate that using spatially-varying precipitation forecasts from high-resolution weather models may be useful for identifying the areas of greatest debris-flow risk. This may be particularly true near large fires or fire complexes where the large scale requires the best possible risk management decisions to be made in order to save lives.

Supervised Classification

The supervised classification methodology from this study provided interesting results between different classifiers and the number of classes. A maximum likelihood classifier was initially used with 4 classes, but the over-representation of the urban class resulted in many incorrect urban pixels in the mountains (Figure 9 top). This led to the inclusion of a 5th class to represent soil/NPV. The addition of the soil/NPV class greatly reduced the amount of urban pixels in the mountains and properly classified many of these pixels as soil/NPV (Figure 9 middle) -- which was the primary goal of adding the new class. From the whole-image perspective, it is very difficult to notice a significant difference in results between the 5-class maximum likelihood and NN classifiers. However, close examination indicates that the NN appears to have a sharper coastline and fewer soil/NPV pixels mixed into the burn area (Figure 9).

Looking at zoomed-in windows from various portions of the larger scene allows for differences among the classifiers to stand out. Figure 10 shows each classifier next to a SWIR image for 3 different regions. The first region, covering Montecito and the nearby mountains, shows that the maximum likelihood classifiers have too many urban (4-class) and soil/NPV (5-class) pixels in the canyons of the Thomas Fire burn region (Figure 10 top). The 5-class NN classifier appears to have done a better job of placing burned pixels in this region. It also has a much sharper coastline compared to the max likelihood classifiers, which smear urban pixels further into the ocean. The middle row of Figure 10, shows an agricultural field to the east of Ventura. This image demonstrates the over-representation of urban pixels in bare agricultural fields by the 4-class max likelihood classifier. The 5-class max likelihood improves upon this by correctly categorizing many of those pixels as soil/NPV. The NN, on the other hand, incorrectly classifies some of these bare agricultural fields as burned areas, while also leaving some of the mountainous shadows in the bottom-right of the image as unclassified pixels. Finally, the

bottom row shows a mountainous region to the northwest of the Montecito area. Interestingly, the Gibraltar Reservoir in the bottom-left corner is not detected by the max likelihood algorithms, but the NN classifier did a very good job of identifying it (Figure 10 bottom). This region also demonstrates the over-classification of urban pixels in the 4-class max likelihood and the conversion to soil/NPV when the 5th class is added. The NN has more cohesive results due to fewer erroneous urban pixels, but also over-classifies burned pixels in this region, which was not affected by the Thomas Fire.

Accuracy results based on reference ROIs indicate that the 3 classifiers performed very similarly (see Table 4 below). Each had an overall accuracy near 98% and Kappa coefficient near 0.96-0.97. Objectively, the 4-class maximum likelihood classifier performed the best with the 5-class NN second. These accuracy numbers are very high and appear to conflict somewhat with the subjective observations discussed earlier. Some limitations of these results will be discussed below.

Measure/Name	4-Class Max	5-Class Max	5-Class NN
Overall Accuracy	98.45%	97.22%	98.20%
Kappa Coefficient	0.9751	0.9591	0.9735

Table 4: Overall accuracy and Kappa coefficient for each classifier

The results for User's and Producer's Accuracy are also shown in Table 5 and 6 below. Many of the class confusion trends that were identified subjectively are also indicated in these tables. For example, pixels classified as urban by the 4-class max likelihood classifier were accurate only 89% of the time (Table 5), the lowest for all classes. Similarly, pixels classified as soil/NPV by the 5-class max likelihood scheme were only accurate 81.9% of the time, with many burned pixels incorrectly classified as soil/NPV (9.6%, not shown). For the NN, soil/NPV areas were often misclassified as burned, leading to a Producer's accuracy of 85.2% (Table 6).

User's Accuracy/Name	4-Class Max	5-Class Max	5-Class NN
Burn Area	98.37%	98.09%	93.56%
Vegetation	99.66%	99.45%	99.69%
Water	100.00%	100.00%	100.00%
Urban	89.01%	96.85%	96.91%
Soil/NPV		81.87%	98.61%
Average	96.76%	95.25%	97.75%

Table 5: User's accuracy for each classifier

Producer's Accuracy	4-Class Max	5-Class Max	5-Class NN
Burn Area	95.67%	89.83%	99.65%
Vegetation	95.92%	95.52%	98.35%
Water	99.98%	99.98%	100.00%
Urban	99.52%	98.18%	98.77%
Soil/NPV		99.17%	85.17%
Average	97.77%	96.54%	96.39%

Table 6: Producer's accuracy for each classifier

One possible reason for the high overall accuracy and Kappa coefficient results of all 3 classifications is likely the chosen reference ROIs. As stated previously, the reference ROIs were independent of the training ROIs, but selected as relatively clean, unambiguous samples. Though well beyond the scope of this study, these samples ideally would have been selected at random and verified in the field (at the time the imagery was taken) to determine their true reference class. However, time and financial constraints precluded this option. The “unambiguous” reference ROIs were chosen partly due to the difficulty of distinguishing land cover classes, such as soil/NPV from brightly reflective vegetation, in some portions of the Sentinel-2 imagery. If more complex reference ROIs were used, the overall accuracy of each classifier would likely be lower. This might be particularly true for the 4-class maximum likelihood classifier, which was subjectively shown to perform poorly in the mountains with far too many urban pixels. Both max likelihood classifiers also struggled with water, completely missing the Gibraltar Reservoir. This feature was not a part of the reference ROIs, but it would have clearly hurt the accuracy scores of the max likelihood classifiers if it was included in the reference ROIs. The max likelihood classifiers also incorrectly mixed urban pixels into the ocean along the California coast. The NN, however, was not without fault of its own. Subjective analysis indicated that it over-classified burned pixels and left more unclassified pixels than the other classifiers. It also took nearly 100 times longer to run than the maximum likelihood classifiers.

Conclusions

As a whole, this study provided promising results for a variety of applications. Using Sentinel-2 imagery to calculate dNBR showed to be an effective method for identifying burned areas and classifying burn severity of the Thomas Fire. The change detection approach using dNBR to monitor burn severity also indicated that it was capable of detecting regrowth in a period of just two months for mildly burned areas. This method also demonstrated some challenges, with time-of-year and sun angle differences apparently producing erroneous areas where burn severity worsened.

The combination of dNBR with terrain, soil properties, and rainfall data also proved useful in predicting debris-flow probability for the Thomas Fire area, answering the first research question. The USGS logistic regression method introduced by Staley et al. in 2016, accurately

quantified this threat for the Montecito area using both observed rainfall amounts and the uniform threshold of 6 mm in 15 min. Further, the spatially-varying precipitation forecasts from the HRRR model also added value by identifying the areas of greatest debris-flow risk (research question 2). This novel approach warrants additional study with the inclusion of an ensemble model to quantify uncertainty and improve consistency. The USGS debris-flow probability model appears to provide a methodology that could potentially be extended to other parts of the world, though some regional modification to the empirical constants would likely be required.

Finally, supervised classification is shown to be an effect method for categorizing pixels (including burned areas) of Sentinel-2 imagery. Increasing the number of classes from 4 to 5 demonstrated subjective improvements for the maximum likelihood techniques. Additional improvements were gained using a NN algorithm, such as a more cohesive burned area and cleaner coastlines, but at the cost of increased compute time and over-classification of burned pixels. Further work to optimize the NN parameters and training ROIs would likely lead to even better results.

References

- Brewer, D., et al., 2005. Classifying and Mapping Wildfire Severity: A Comparison of Methods, *Photogrammetric Engineering & Remote Sensing*, 71(11): 1311-1320.
- Eidenshink, J.; Schwind, B.; Brewer, K.; Zhu, Z.; Quayle, B.; Howard, S. 2007. A project for monitoring trends in burn severity. *Fire Ecology*. 3(1): 3-21.
- Melillo, J. M., et al., 2014. Climate change impacts in the United States: The third national climate assessment. *U.S. Global Change Research Program*.
- National Weather Service, Los Angeles. 2018. NWS Los Angeles Twitter Page.
<https://twitter.com/NWSLosAngeles/status/950785251520995333> (last accessed 10 April 2018).
- National Weather Service California Nevada River Forecast Center. 2018. NWS CNRFC Twitter Page. <https://twitter.com/NWSCNRFC/status/951127915013509121> (last accessed 10 April 2018).
- Staley, D. M., et al., 2016. Prediction of spatially explicit rainfall intensity-duration thresholds for post-fire debris-flow generation in the western United States, *Geomorphology*, 278: 149-162.
- Thomas Fire Watershed Emergency Response Team: Final Report. 26 February 2018. *Cal Fire*, 1-241.



Figure 1: Photos from Santa Barbara County Fire-Public Information Officer Twitter: @EliasonMike, SBCFireInfo

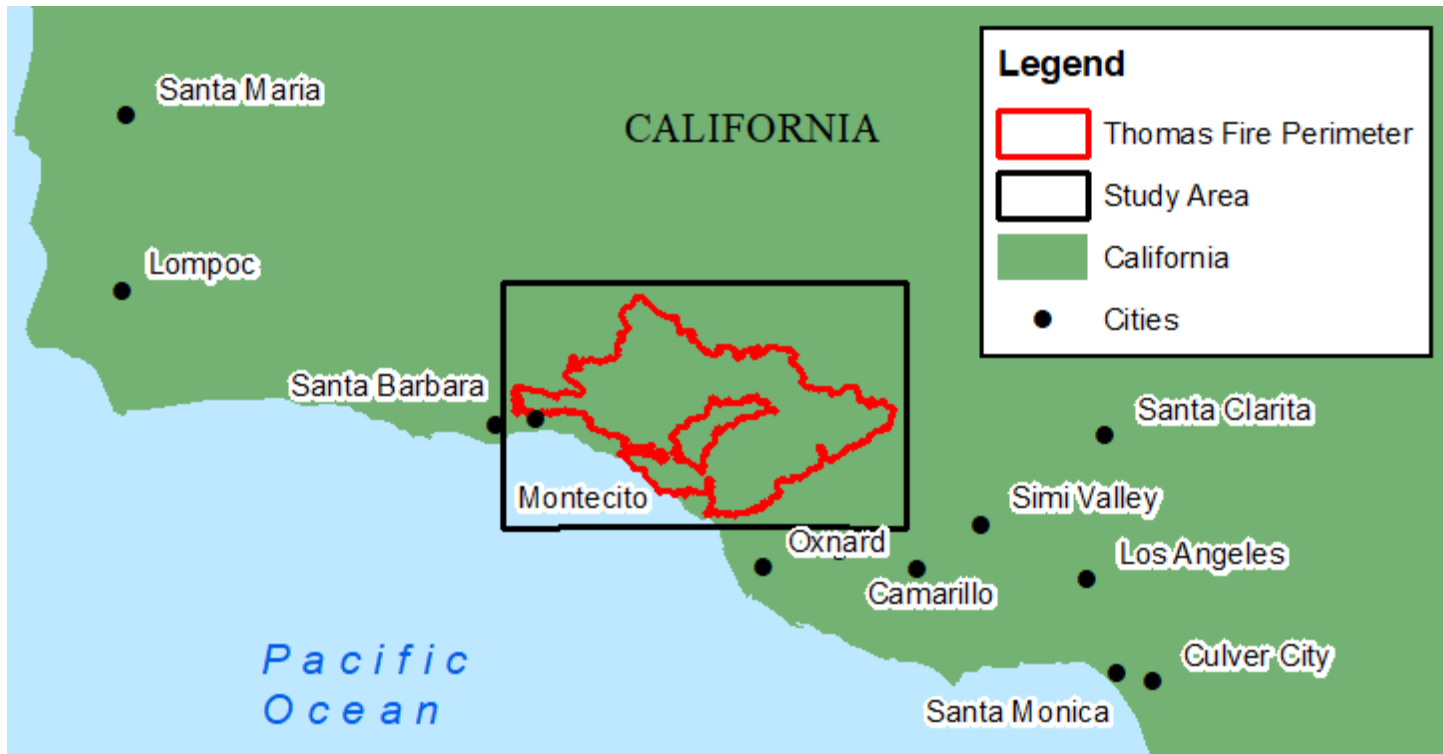


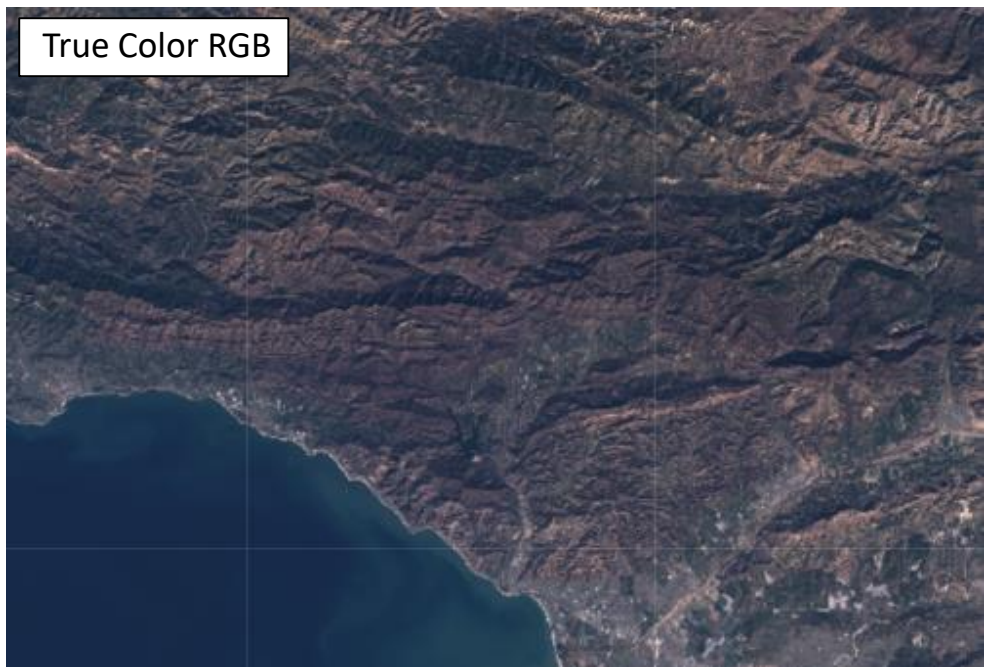
Figure 2: Thomas Fire perimeter and primary study area

True Color RGB Image:

Red = Band 4 (red)

Green = Band 3 (green)

Blue = Band 2 (blue)



False Color NIR Image:

Red = Band 8A (red edge 4)

Green = Band 4 (red)

Blue = Band 3 (green)



False Color SWIR Image:

Red = Band 12 (SWIR 2)

Green = Band 8A (red edge 4)

Blue = Band 4 (red)

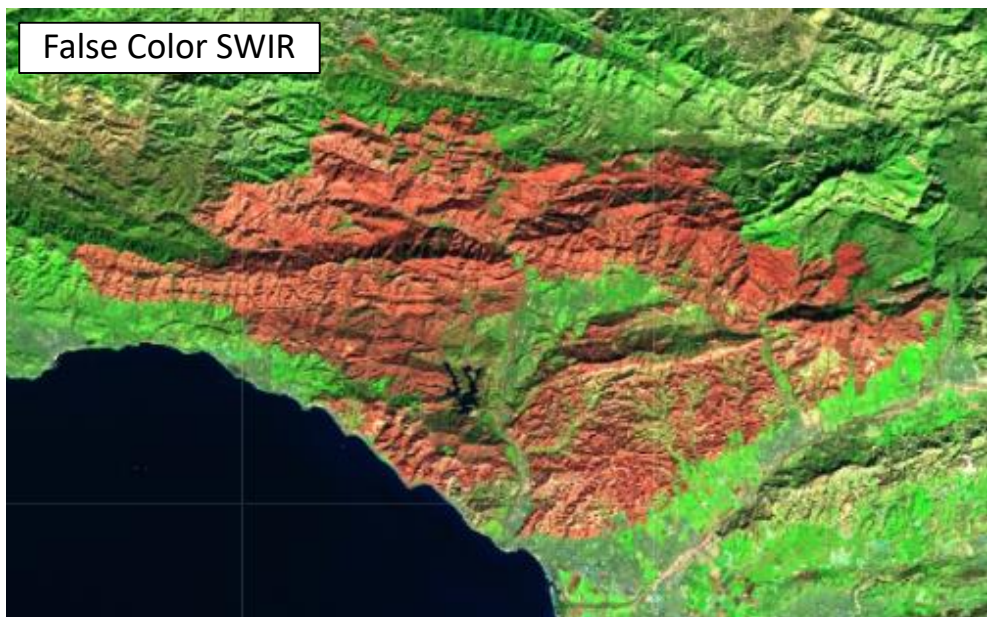
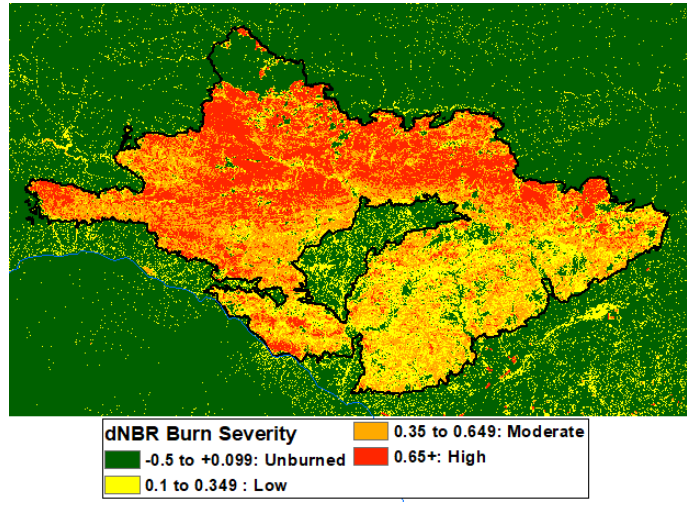
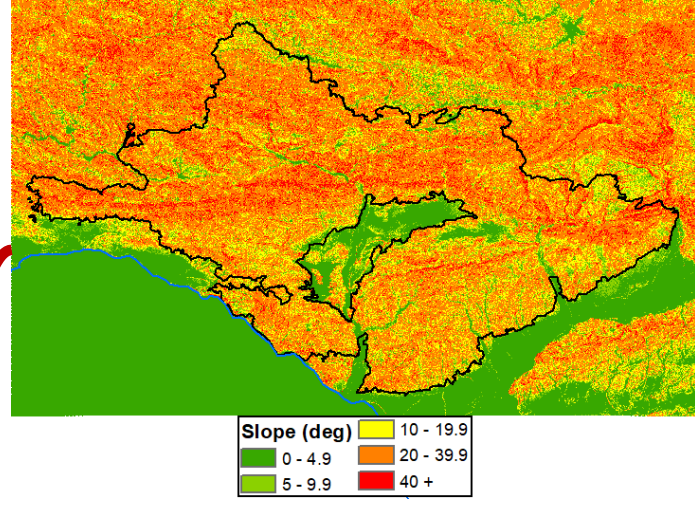


Figure 3: Sentinel-2 MSI imagery from 22 January 2018

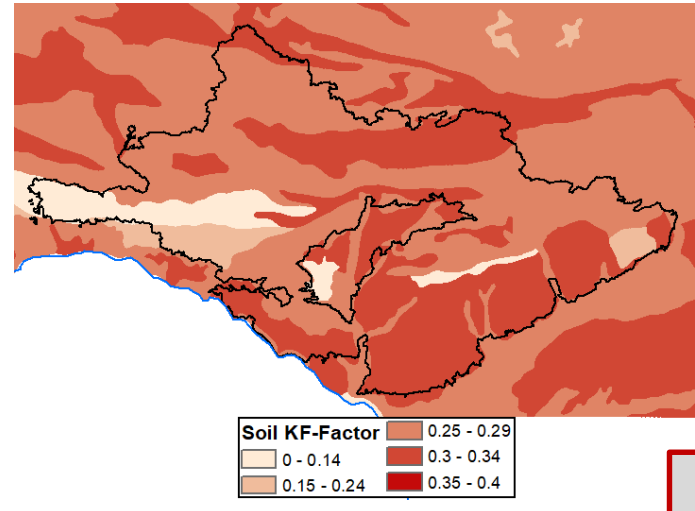
Difference Normalized Burn Ratio



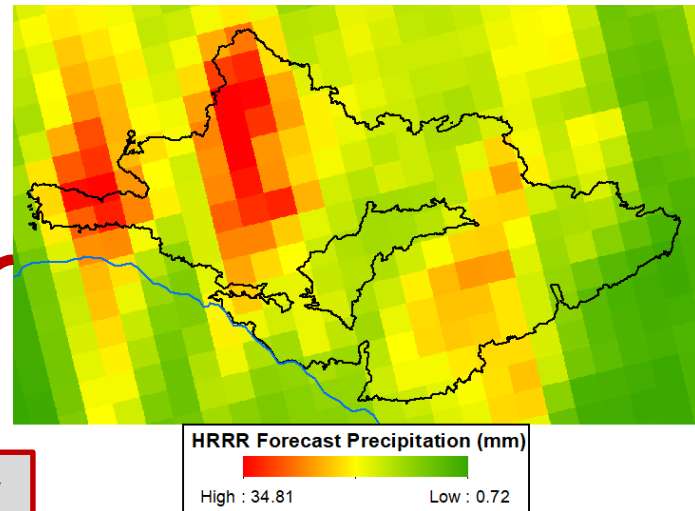
Slope Analysis



Soil Erodibility: KF-Factor



HRRR 1-Hour Forecast Precipitation



Average by
Watershed

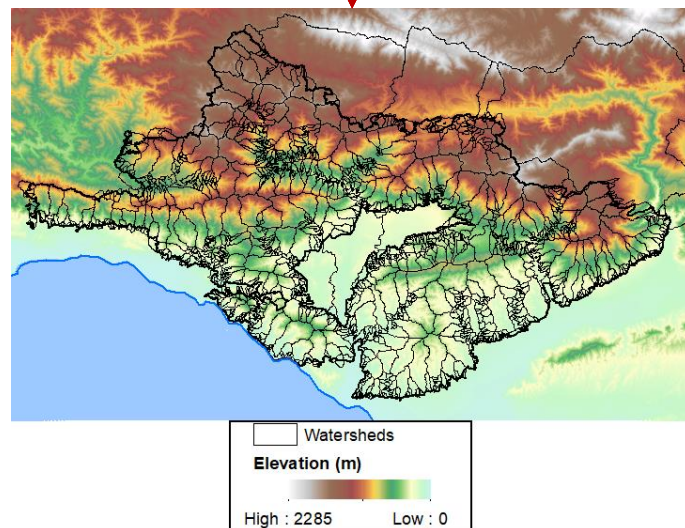


Figure 4: Diagram of debris-flow probability calculation methodology

Pre-fire SWIR Image: 03 Dec 2017



Post-fire SWIR Image: 22 Jan 2018



dNBR Image: preNBR – postNBR

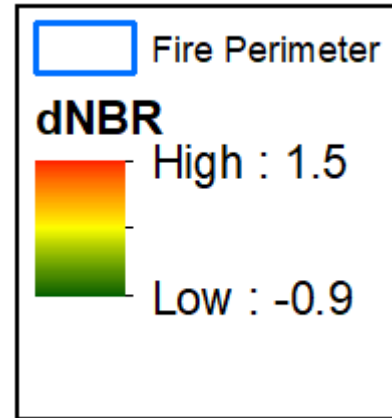
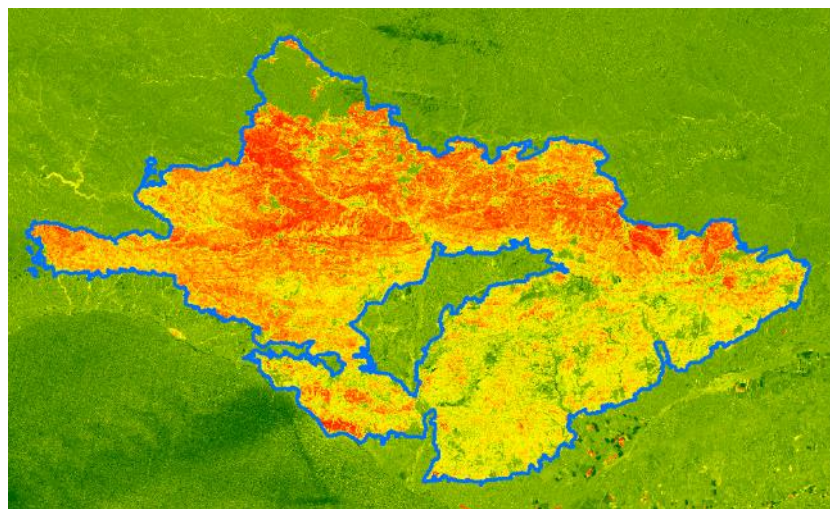


Figure 5: Pre- and post-fire SWIR imagery and dNBR image

dNBR change from 22 Jan to 28 Mar 2018

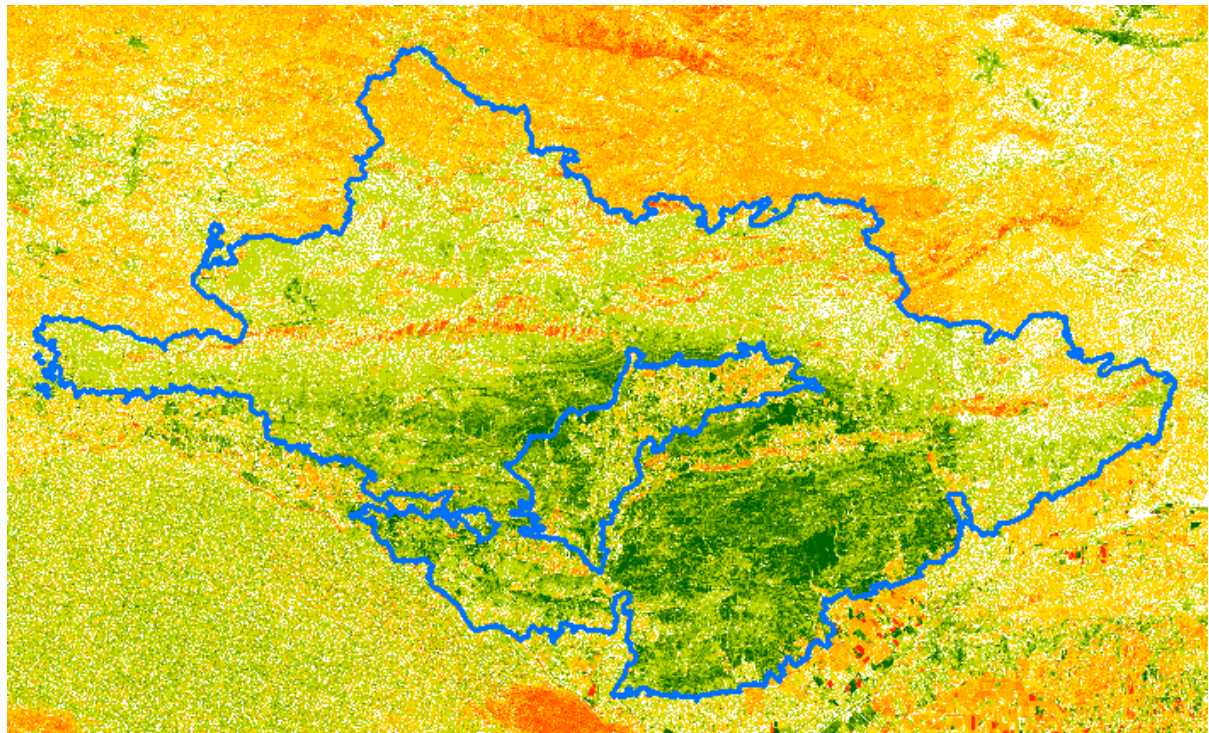
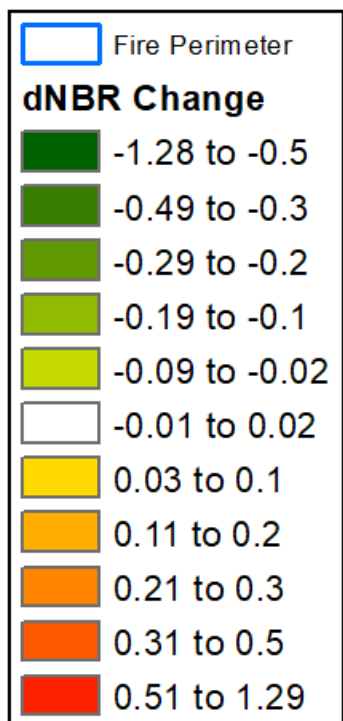
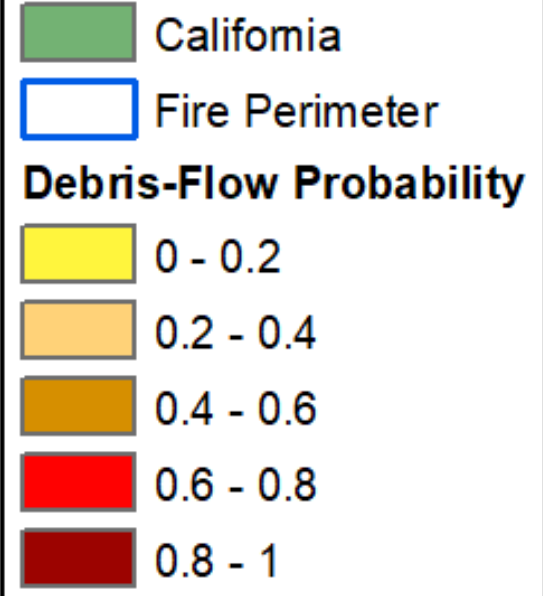
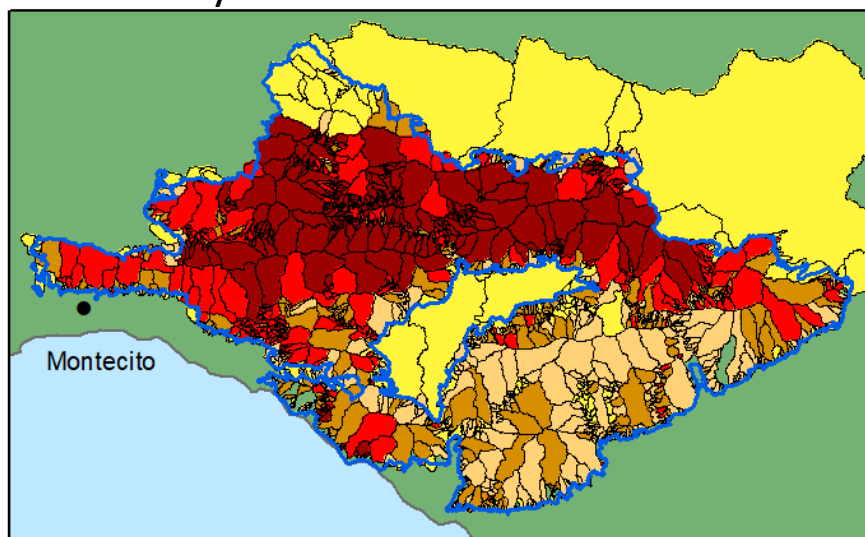
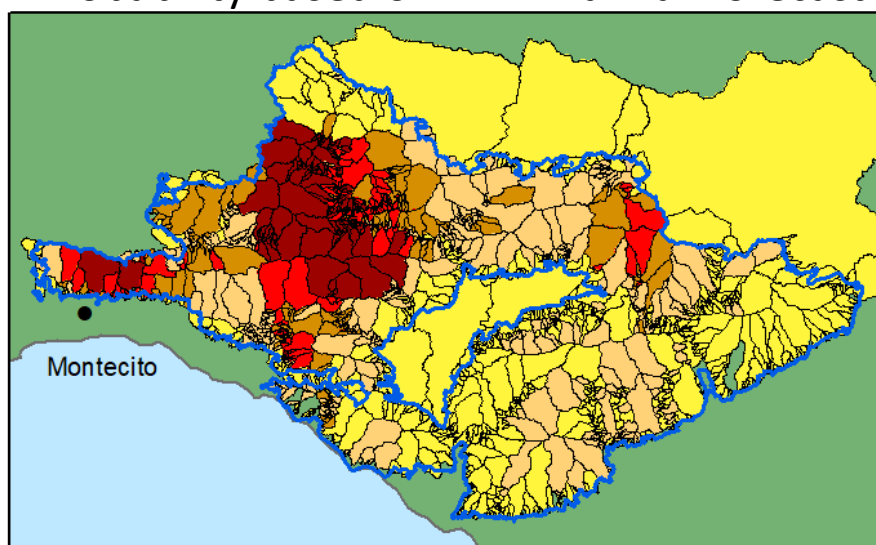


Figure 6: dNBR change detection taken approximately 9 weeks apart

Probability based on uniform 6 mm rainfall



Probability based on HRRR rainfall forecast



Probability difference (HRRR – uniform)

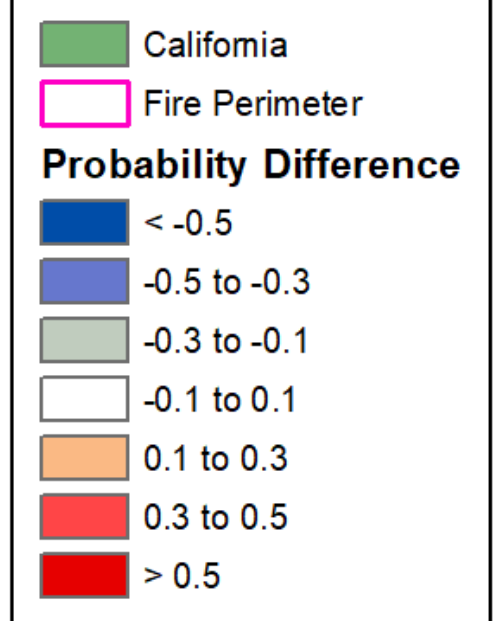
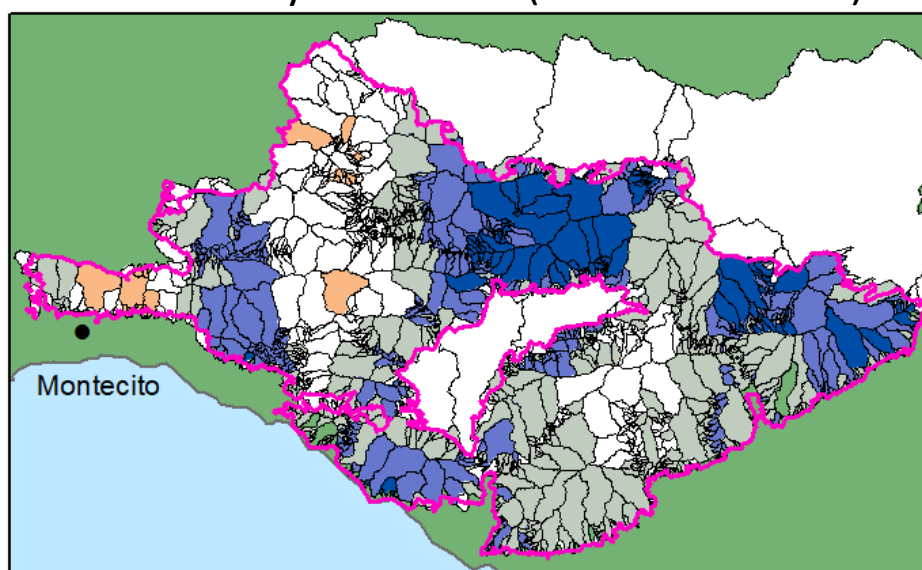


Figure 7: Debris-flow probability results from uniform rainfall, HRRR rainfall forecast and difference (HRRR – uniform)

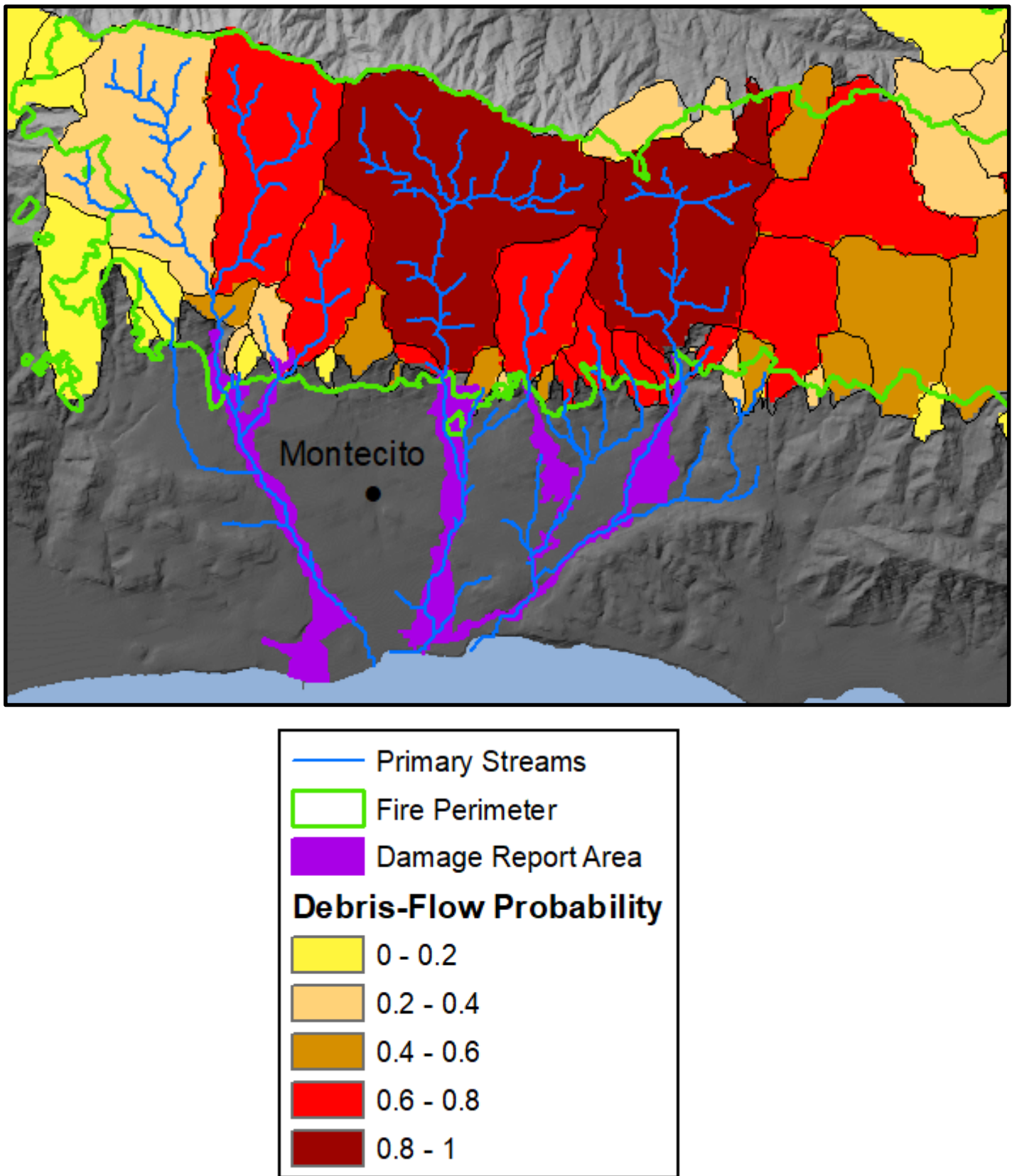


Figure 8: Zoomed-in view of debris-flow probability in the Montecito area with the primary streams and damage report area identified

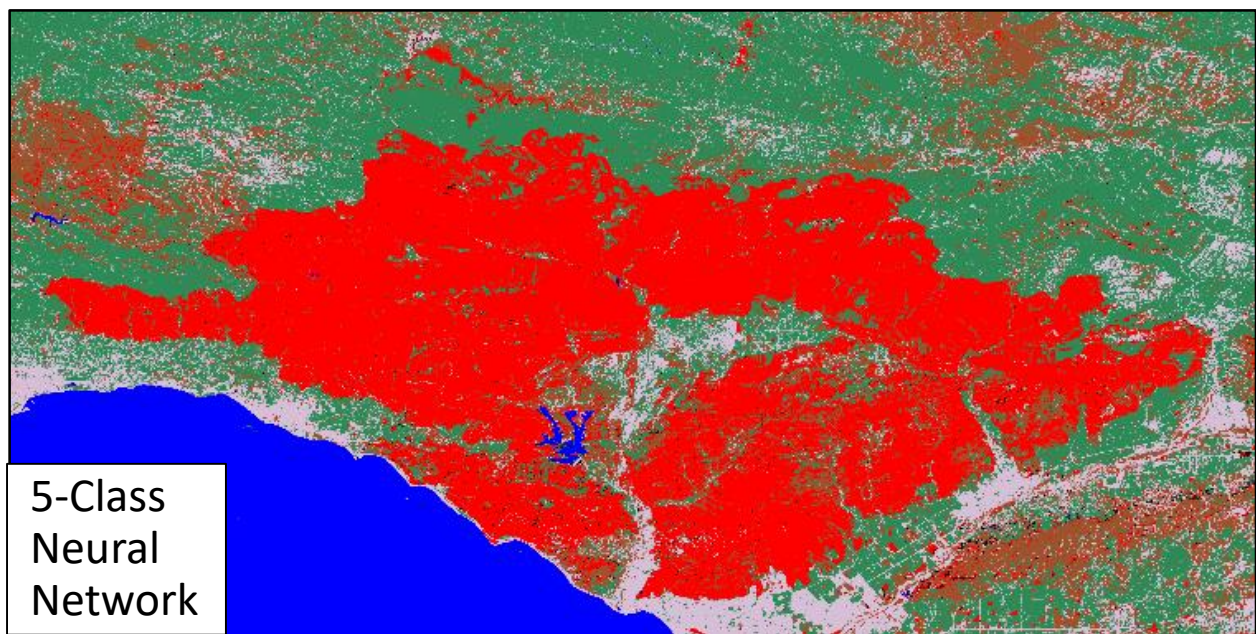
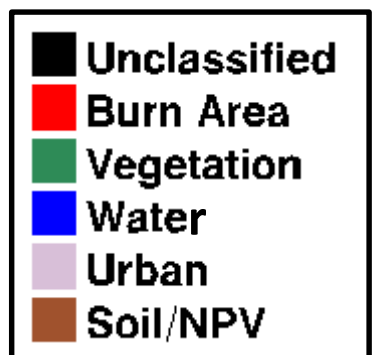
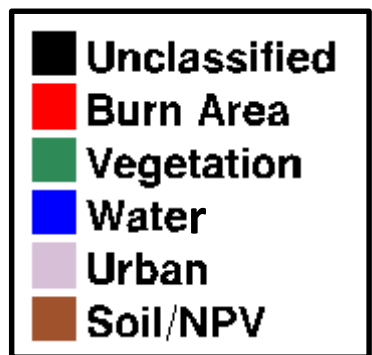
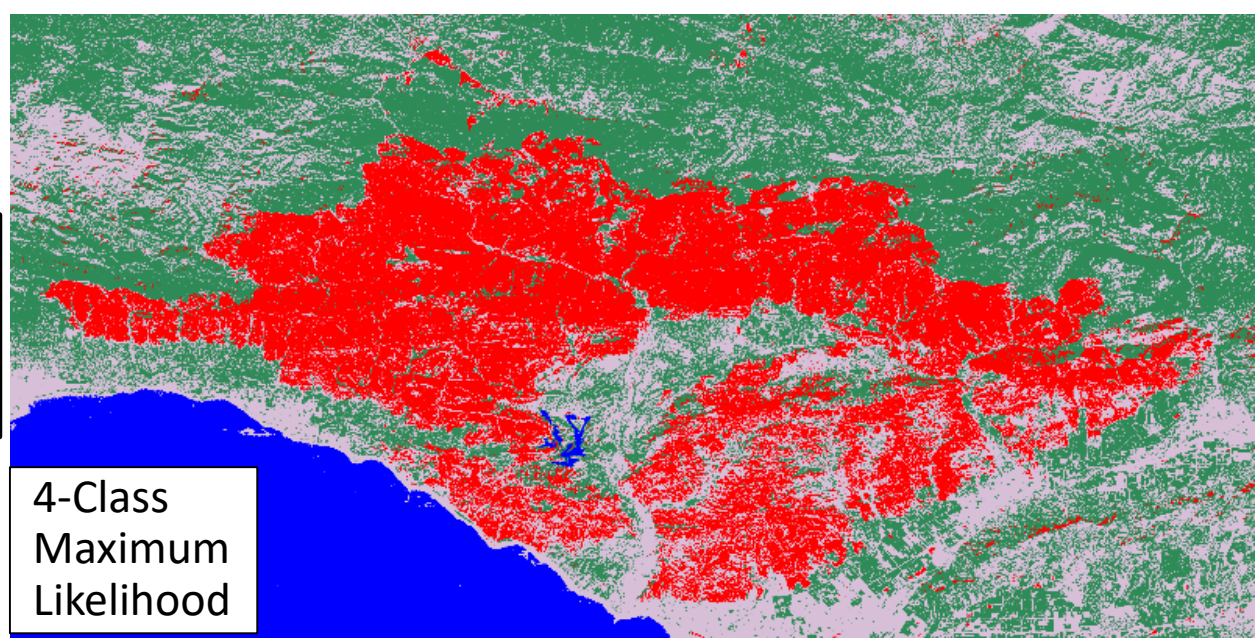


Figure 9: Classification results from 4-class maximum likelihood (top), 5-class maximum likelihood (middle) and 5-class neural network (bottom)

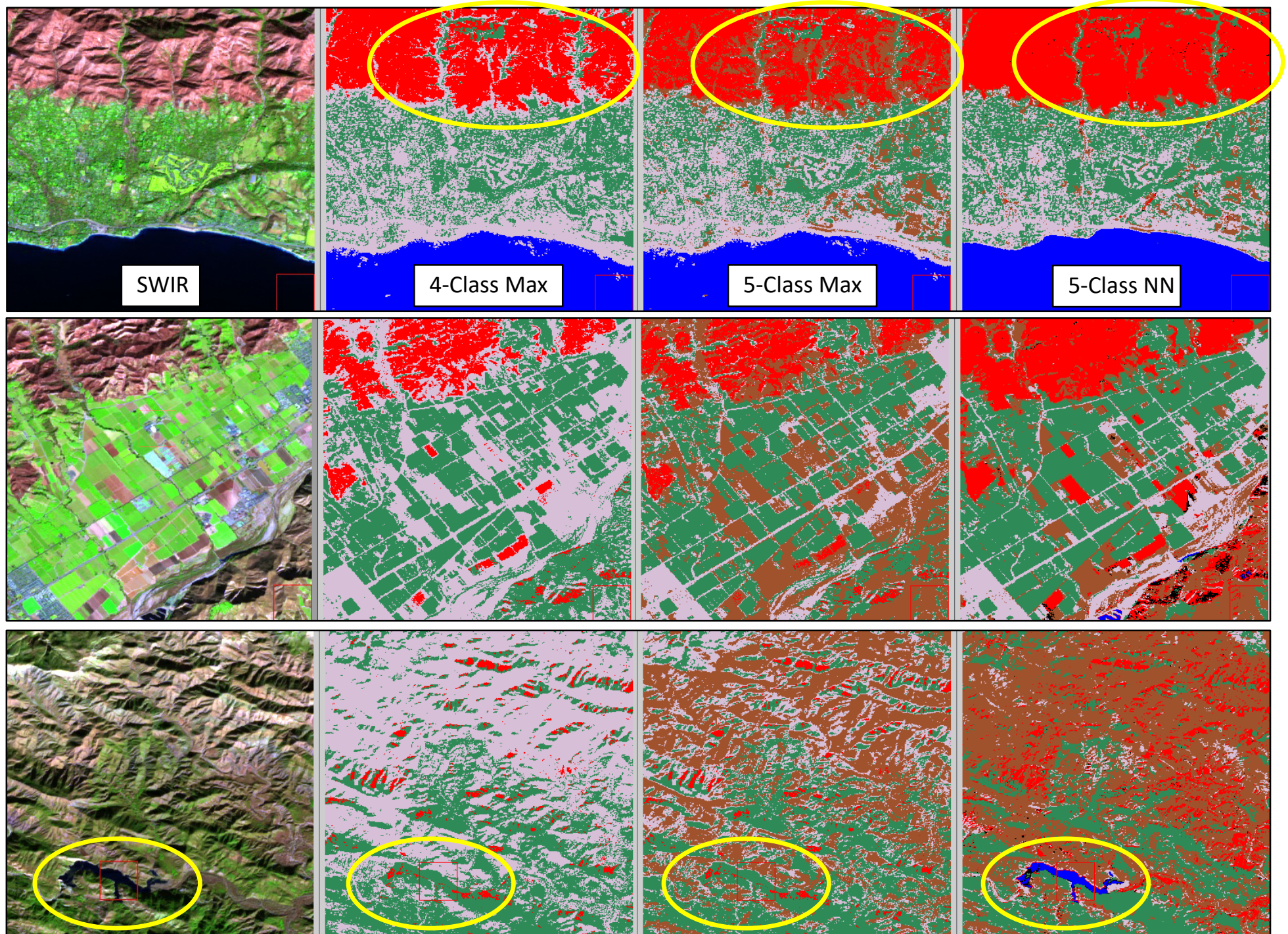


Figure 10: Zoomed-in classification results from Montecito area mountains (top row), agriculture east of Ventura (middle row), and mountains NW of Montecito (bottom row). The first column is a SWIR image, second column is 4-class maximum likelihood, third column is 5-class maximum likelihood, and fourth column is 5-class neural network.